Effect of Tartrazine on Adrenal Cortex of Adult Male Albino Rat and the Possible Protective Role of Argan Oil (Histological and Biochemical Study)

Original Article

Amira Ibrahim El-Masry[1], Gehan Mohamad Soliman[2], Sadika Mohamad Tawfik[2] and Suzan Elsayed Abo Elnasr[2]

Department of Histology and Cell Biology, Faculty of Medicine, [1]Suez University, [2]Tanta University, Egypt

ABSTRACT

Background: Tartrazine (TRZ) is one of the most frequently used coloring compounds in the food and pharmaceutical industries. Extensive usage of tartrazine leads to multi-system disorders in rodents and humans. Argan oil (AO) has been shown to have antioxidant properties.

Aim of the Work: To evaluate the effect of TRZ on the adrenal cortex of adult male albino rat and the possible protective role of AO.

Materials and Methods: Forty adult male albino rats were divided into four groups equally. Group I (control group). Group II received AO at an oral dose of 5 ml/kg once daily for four weeks. Group III received TRZ at an oral dose of 300 mg/kg dissolved in 1 ml of distilled water once daily for four weeks. Group IV received TRZ in concomitant with AO in the same dose and manner as Groups II&III. Blood samples were taken to measure the serum hormonal levels of aldosterone, corticosterone, cortisol and DHEA-S. The adrenal glands were processed for histological, immunohistochemical, and transmission electron microscope (TEM) study.

Results: Group III revealed disturbed architecture of the three adrenal cortical zones linked with deposition of collagen fibers in the capsule and in-between the cells in Masson's trichrome stained sections with intense positive immune reaction to cleaved caspase 3. Electron microscopic examination revealed indented irregular nuclei with perinuclear space dilation and swollen mitochondria. AO intake ameliorated the histological, immunohistochemical, biochemical, and morphometric results.

Conclusion: Co-administration of AO with TRZ alleviated the harmful effects of TRZ on the adrenal cortex.

Key Words: Adrenal cortex, argan oil, cleaved caspase 3, histopathology, tartrazine.

Received: 30 September 2024**, Accepted:** 12 November 2024

Corresponding Author: Suzan Elsayed Abo Elnasr, Department of Histology and Cell Biology, Faculty of Medicine, Tanta University, Egypt, **Tel.:** +2 010 0074 8926, **E-mail:** souzan.emamo@med.tanta.edu.eg

ISSN: 2735-3540, Vol.75, No. 4, December 2024

INTRODUCTION

The usage of synthetic food dyes has increased in the last few years. Food colors can affect the perception of flavor, palatability, and acceptability through visual tasting. They are added to various items to improve their aesthetic appeal or compensate for natural and/or technological variations. To achieve this, the food business mostly uses artificial dyes[1,2].

Azo dyes are the most widely used artificial dyes in the world. Their diverse and brilliant colors are a result of their structural chemical diversity. They have no odd taste or odor. Also, they are affordable, accessible, stable, and uniform. Compared to brown dyes, yellow and red dyes are more commonly utilized in the food business[3].

One of the most widely used food colorings is tartrazine (TRZ), also known as E 102, FD, and C Yellow. It is yellowish in color and is available in granular or powder form. Due to its low cost, tartrazine is desirable and commonly utilized in many products. It has been widely used in the food business, the leather, cosmetics, and fabrics sectors, as well as in the manufacture of medicinal capsules for vitamins and acid-reducing agents, particularly in developing nations[4,5].

When used within the acceptable daily intake (ADI) range, artificial food colorings like TRZ are considered safe. Children are the biggest users of colored food products, especially in underdeveloped nations, thus they are at significant risk because they frequently consume

DOI: 10.21608/ASMJ.2024.324628.1321

more than the recommended ADI[6]. Several disorders such as behavioral changes, hypersensitivity reactions, teratogenicity, gastrointestinal, renal, endocrinal, and hematological disorders have been associated with tartrazine use[7], but little is known about the effect of it on the adrenal cortex. Therefore, our study aimed to demonstrate the possible histopathological effects of TRZ on the suprarenal cortex.

Argan oil (AO) is extracted from the kernel of the argan tree [Argania spinosa (L.) Skeel; Sapotaceae], which is one of the oldest endemic forest trees in southwestern Morocco and Algeria. The chemical constituents of argan oil make it one of the highest-quality plant seed oils with a high nutritional and dietetic value[8].

Edible AO is used for medicinal and food nutritional purposes. Argan oil has a low smoking point and is very versatile to cook, marinate, bake, or finish with. It is consumed as a dip with crusty bread and drizzled over couscous, vegetables, salads, eggs, fish, tagines, and others[9].

Fatty acids, such as polyunsaturated fatty acids (PUFA), monounsaturated fatty acids (MUFA), and saturated fatty acids, are the primary chemical constituents of Argan oil. Many other compounds are also present like carotenes, tocopherols, phenols, sterols, squalene, and xanthophylls. All these components make AO a rich source of antioxidants[10] so we also aimed to show how AO can protect the suprarenal cortex from the possible TRZ-induced damage effects.

AIM OF THE WORK

To study the biochemical and histological effects of tartrazine on the adrenal cortex of adult male albino rat and the possible protective role of argan oil.

MATERIALS AND METHODS

The experimental procedure was conducted in the department of Histology and Cell Biology, Faculty of Medicine, Tanta University.

Animals

Forty adult male albino rats (200 to 250 gm) were involved in the current study. Throughout the experiment aged 3 months, the rats were housed at a laboratory temperature of 22±23°C with normal light/dark cycles. Each animal received an identical normal laboratory diet (ad libitum) and had unlimited access to food and water in appropriately clean, well-ventilated cages.

Chemicals

1. **Tartrazine:** molecular formula (C16H9N4Na3O9S2), was purchased from Loba Chemie (India) through El-Gomhouria Company for Trading Chemicals and Medical Appliances, Cairo, Egypt, in the form of powder with a purity of about 87%.

2. **Argan oil:** was purchased from the local market in Jeddah, KSA. It was kept in a cool and dark place to avoid oxidation.

Experimental design

The rats were divided equally into four groups, (n=10 per group):

Group I (control group): The rats were subdivided into two equal subgroups (n=5):

- Subgroup IA: The rats were kept without any treatment until the end of the experiment for the histological studies of the normal adrenal cortex.

- Subgroup IB: Each rat received 1ml of distilled water (the solvent of TRZ) by a gastric tube once daily for four weeks.

Group II (AO group): Each rat was administered 5ml/kg of argan oil[11] by a gastric tube once daily for four weeks, using a flexible ball tip needle connected to an insulin syringe to determine the appropriate dose.

Group III (TRZ group): This group received 300 mg/kg of TRZ dissolved in 1 ml of distilled water by a gastric tube once daily for four weeks. The used TRZ dose represents 5% of the LD50 (TRZ- LD50 corresponds to 6375 mg/kg when orally administered in rats)[12].

Group IV (TRZ + AO): This group received TRZ in concomitant with AO in the same dose and manner as groups II & III once daily for four weeks.

At the appropriate time (on the day 29 from the start of the experiment), the rats were fasted overnight, and

sodium pentobarbital (50 mg/kg) was administered intraperitoneally to each animal for anesthesia[13]. Two milliliters (2 mL) of blood were withdrawn from each rat by cardiac puncture via the left ventricle using a 23–25-gauge needle slowly to prevent heart collapse. The blood was placed in sterile vacutainers with a clot activator and was left to clot for 20 minutes. Then an immediate incision was made in the abdominal wall and the suprarenal glands were dissected and each gland was divided carefully into two specimens. One half underwent light microscopy processing, whereas the other half underwent transmission electron microscopy processing. Disposal of the sacrificed animals was consistent with the health and environmental concerns to ensure no environmental pollution; they were sent in a special package to be incinerated in Tanta Faculty of Medicine general incinerator.

Biochemical analysis

After blood samples collection, serum was then separated by centrifugation at 3000 revolutions per minute (rpm) for 15 minutes. The sera were aliquoted and stored at –80°C until evaluation for the levels of aldosterone, corticosterone, cortisol and dehydroepiandrosterone sulfate (DHEA-S). Prior to analysis, frozen samples were thawed and brought to room temperature. Serum hormones were performed on Cobas e-411 (Roche Diagnostic -Indiana, United States): Fully automated, sample-oriented, random access, Electrochemiluminescence immunoassay system. The mean hormonal levels of aldosterone, corticosterone, cortisol, and DHEA-S were assessed in the different studied groups.

Preparation of samples for Histological study

A- Light microscopic studies

For histological examination, the adrenal gland samples were fixed in a 10% buffered formalin solution for 24 hours then dehydrated in ascending grades of ethanol. Embedding paraffin was the last step, followed by cutting serial sections of 5 μm thickness. All the sections were subjected to:

1. Routine hematoxylin and eosin (H&E) stain to assess the histological structure of the adrenal cortex[14].

2. Masson's trichrome stain for collagen fiber demonstration[15].

3. Immunohistochemical stains for detection of cleaved caspase-3[16].

Adrenal gland sections (5-μm-thick) were deparaffinized and hydrated. Block endogenous peroxidase activity was done using 3% H_20_2. The citrate buffer was utilized for antigen retrieval after the treatment of the sections in a microwave. Overnight at room temperature was the accurate duration for incubation of the tissue sections with a diluted primary antibody that was applied to the sections for 2 hours and was directed against cleaved caspase-3; a rabbit polyclonal antibody (Cat. No GB11532, Service bio, Wuhan, China, 1:500 dilution), Biotinylated polyvalent secondary antibody (Cat. No. G1214, Service bio, Wuhan, China, 1:200 dilution) was the detection method for use in the second step of staining. The last step was staining the sections with diaminobenzidine (DAB) solution (as chromogen) for 5–10 min, washing them three times in phosphate buffered saline (PBS) for 2 min each, and counterstaining with Mayer hematoxylin. Finally, the slides underwent dehydration, clearing, and xylene mounting. Negative control section was applied by the same method with replacement of the primary antibody with PBS. The positive control was human stomach cancer.

All specimens were examined and photographed using Olympus light microscope (Tokyo, Japan) attached to an Olympus digital camera (DXC1850P, Tokyo, Japan) in Histology and Cell Biology Department, Faculty of Medicine, Tanta University.

B-Transmission electron microscopic (TEM) study

The specimens followed routine processing, including 2.5% phosphate-buffered glutaraldehyde preservation and epoxy resin embedding. Toluidine blue dye was used in semithin slices (1 μm thick) to select the areas for TEM studies. On 200 mesh uncoated copper grids, 75-nm thick ultrathin slices were selected, dyed with uranyl acetate, and then counter-stained with lead citrate[17]. The specimens were subsequently photographed using a JEOL-JEM -100 SX electron microscope at Electron Microscopic Unit, Faculty of Medicine, Tanta University, Egypt.

C-Histo-morphometric study

Morphometric studies were performed using image J (Version 1.53t 24) software (National Institute of Health, Bethesda, Maryland, USA), at magnification X 400. Ten separate nonoverlapping fields were chosen randomly from each slide of each group for quantitative evaluation of the following parameters[18]:

I. The mean area percentage of collagen fibers (in Masson's trichrome-stained sections) of the different study groups.

II. The mean area percentage of immune reaction to cleaved caspase -3 (in the DAB-stained slides) of the different study groups.

D-Statistical analysis

The data were statistically analyzed using SPSS software version 20 (SPSS Inc., Chicago, IL, USA), then compared by one-way analysis of variance (ANOVA) to create statistical analyses before using Tukey's test to compare all groups. The mean and standard deviation were used to represent the entire set of data. The differences were regarded as statistically significant if the probability value (*P-value*) was less than 0.05, highly significant if *P-value* was less than 0.001, and non-significant if *P-value* was greater than 0.05[19].

Ethical Consideration

Protocols and experimental design were carried out in accordance with Tanta University's Institutional Animal Care and Use Committee (TU-IACUC) requirements. Code of approval for the ethical committee: 36203/12/22.

RESULTS

General observation

Throughout the study, the control group rats were awake and alert while the rats of TRZ group appeared feeble and lethargic and gradually improved subsequent to AO supplementation. No mortality was recorded in the animals during the experimental period.

Histological examination of the adrenal gland specimens

All the subgroups of group I (Control) and group II (AO) showed almost the same histological structure in LM and TEM.

Light microscopic results

H & E stained- sections

Control & AO groups (Group I&II): The examined suprarenal cortex sections obtained from groups I &II were identical and demonstrated the apparent normal structure of the suprarenal gland. A capsule of connective tissue (CT) encircled the adrenal gland that was composed of an outer cortex and an inner medulla. The adrenal cortex was divided into three concentric zones, outer zona glomerulosa (ZG), middle zona fasciculata (ZF), and inner zona reticularis (ZR) (Figure 1A). Zona glomerulosa cells were situated at the outer part of the cortex, directly below the capsule of CT. The cells were arranged in closely packed ovoid clusters and arches of columnar cells that were separated by trabeculae of CT. The cells had acidophilic vacuolated cytoplasm and rounded nuclei (Figures 1B,C). Cells of ZF were organized in straight parallel-oriented cell cords. The cords were separated by sinusoidal capillaries. The cells were large polyhedral with distinct boundaries and had faintly eosinophilic vacuolated cytoplasm and rounded vesicular nuclei. Binucleated cells were also seen (Figures 1B,D). Cells of ZR were organized in a network of anastomosing cords. These cords were separated by fenestrated capillaries. The cells were small polyhedral with vacuolated cytoplasm (Figure 1E).

TRZ group (group III): Examination of the suprarenal gland samples of this group showed loss of the normal cellular arrangement in each cortical zone (Figure 2A). The CT capsule was irregular and sloughed in some sections (Figure 2B).

Examination of ZG revealed an irregular cellular arrangement of the glomerulosa cells with apparent hypercellularity in some sections. Deposition of acidophilic material between the disorganized cells, inflammatory cellular infiltrations, and eosinophilic areas with indistinct cell boundaries were also noticed (Figures 2B,C,D,E). Many cells had a highly vacuolated cytoplasm [Figure (2D)]. Moreover, widened intercellular spaces were noticed and an accessory adrenocortical nodule was observed; cells were enveloped by CT with flattened nuclei of fibroblasts and separated by sinusoidal capillaries (Figure 2E). Cells of ZF lost their regular arrangement with indistinct cell boundaries and were observed to have a large ballooned and highly vacuolated cytoplasm. Some cells appeared with faded nuclei, and others with shrunken dark (pyknotic) nuclei. Cells with hyper eosinophilic cytoplasm and lost nuclei were also observed. Moreover, the sinusoidal capillaries appeared dilated with extravasation of blood (Figures (2C,D,E).

Cells of ZR were found to have vacuolated cytoplasm. Some cells appeared with shrunken dark nuclei and others had faded nuclei. Homogeneous eosinophilic material between the cells was also observed (Figure 2F).

TRZ + AO group (group IV): Group IV showed preservation of the cytoarchitecture of the cortical zones (ZG, ZF and ZR (Figure 3A). Cells of ZG, ZF and ZR showed more or less normal histological architecture as the control group, but few cells with faded nuclei in ZF were observed (Figures 3B,C).

Masson's Trichrome-stained sections

Control & AO groups (Group I&II): The adrenal cortex sections of these two groups showed the same histological structure. The collagen fibers in the thin CT capsule and in between the adrenocorticocytes appeared few & regular (Figure 4A).

TRZ group (Group III): Sections of this group exhibited an apparent thick and corrugated CT capsule with excessive irregular collagen fibers in it and in between the adrenocorticocytes (Figure 4B,C).

TRZ +AO group (Group IV): Adrenal cortex sections of group IV displayed fine regular collagen fibers in the CT capsule and in between the adrenocorticocytes (Figure 4D).

Immunohistochemical-stained sections for cleaved caspase-3

Negative control: Microscopic analysis of the adrenal cortex negative control sections revealed abolished cytoplasmic or nuclear reaction in ZG, ZF and ZR (Figures 5 A,B).

Control & AO groups (Group I&II): The adrenal cortex immunostained sections of these two groups revealed no cytoplasmic or nuclear reaction in ZG, ZF and ZR (Figures 6A,B).

TRZ group (Group III): Sections of Group III showed an apparently intense positive cytoplasmic and nuclear immune reactions in ZG, ZF (Figure 6C) and ZR (Figure 6D).

TRZ +AO group (Group IV): This group showed noticeable weak positive cytoplasmic and nuclear immune reactions in ZG, ZF (Figure 6E) and ZR (Figure 6F).

Transmission electron microscopic results

Control & AO groups (Group I&II): Examination of the different ultrathin sections from both groups showed normal ultrastructure of the adrenal cortical cells of the three zones ZG, ZF, and ZR. Cells of ZG had rounded euchromatic nuclei and prominent nucleoli, multiple mitochondria with tubular cristae and variable shapes, varying from elongated to oval or rounded shapes, and few lipid droplets. It had smooth endoplasmic reticulum cisternae (SER), secondary lysosome, and free ribosomes (Figure 7A).

Zona fasciculata cells showed euchromatic spherical nuclei with prominent nucleoli, numerous lipid droplets, lysosomes, SER cisternae, and numerous spherical mitochondria. The adjacent cells were separated by intercellular spaces (Figure 7B).

Examination of ZR showed that cells displayed euchromatic rounded nuclei with prominent nucleoli, numerous mitochondria with tubular cristae, and numerous lipid droplets. SER cisternae and scattered ribosomes were also detected (Figure 7C).

TRZ group (Group III): When the ultrathin sections of this group were examined, notable ultrastructural changes were found. Examination of ZG detected that some cells appeared with a relatively shrunken indented nucleus, while others had a small heterochromatic nucleus with dilatation of the perinuclear cisterna. The cytoplasm contained numerous lipid droplets, dilated cisternae of SER, small mitochondria with tubular cristae and lysosomes. Rarified areas of the cytoplasm were detected. Moreover, widening of the intercellular spaces was also noticed. The fibroblast of the CT capsule appeared with cytoplasmic vacuolation (Figure 8A).

Examination of ZF detected that some nuclei were irregular, and others were shrunken with dilated perinuclear cisterna (Figures 8B,C,D). Nuclear indentation was observed either by lipid droplets (Figure 8B) or by swollen, vacuolated mitochondria with disturbed cristae (Figure 8D). A large number of lipid droplets of varying sizes accumulated, and some appeared coalesced. Dilated SER cisternae, multiple lysosomes, and large areas of cytoplasmic rarefaction were also observed (Figures 8B, C).

Examination of ZR showed that some cells appeared with irregular, indented nuclei and dilatation of the perinuclear cisterna (Figures 8E,F). Cytoplasm contained multiple intact mitochondria of different sizes and shapes, multiple lysosomes, and dilated SER cisternae (Figure 8F). Concerning lipid droplets, there was a collection of variable-sized lipid droplets (Figure 8E). Additionally, areas of rarified cytoplasm with widening of the intercellular spaces were also detected (Figures 8E,F).

TRZ +AO group (Group IV): Examination of ultrathin sections of the adrenal cortex of group IV showed that most cells of the three zones appeared more or less as the control group. Examination of ZG, ZF and ZR detected that the cells appeared with a rounded, regular euchromatic nucleus and prominent nucleolus. The cytoplasm contained an abundance of mitochondria, SER cisternae and lipid

droplets. A few changes were still present as dilatation of perinuclear cisterna of ZF and ZR cells (Figures 9A,B C).

Biochemical analysis, morphometric results and statistical analysis

There was a non-significant difference (p>0.05) between control group and AO group regarding the used parameters.

A- Biochemical results

The mean hormonal levels of aldosterone, corticosterone, cortisol and DHEA-S in group III were highly significantly decreased (*P-value* <0.001) versus groups I, II and IV. Group IV showed a highly significant increase (*P-value* <0.001) compared to group III (Table 1, Figure 10).

B- Morphometric results and statistical analysis

The mean area % of collagen fibers in group III revealed a highly significant increase (*P value* <0.001) compared to groups I, II and IV. Group IV showed a highly significant decrease (*P value* <0.001) compared to group III (Table 2, Figure 11).

The mean area % of cleaved caspase-3 immune reaction in the adrenal cortex in group III showed a highly significant increase (*P value* <0.001) compared to groups I, II and IV. Group IV showed a highly significant decrease (*P value* <0.001) compared to group III (Table 3, Figure 12).

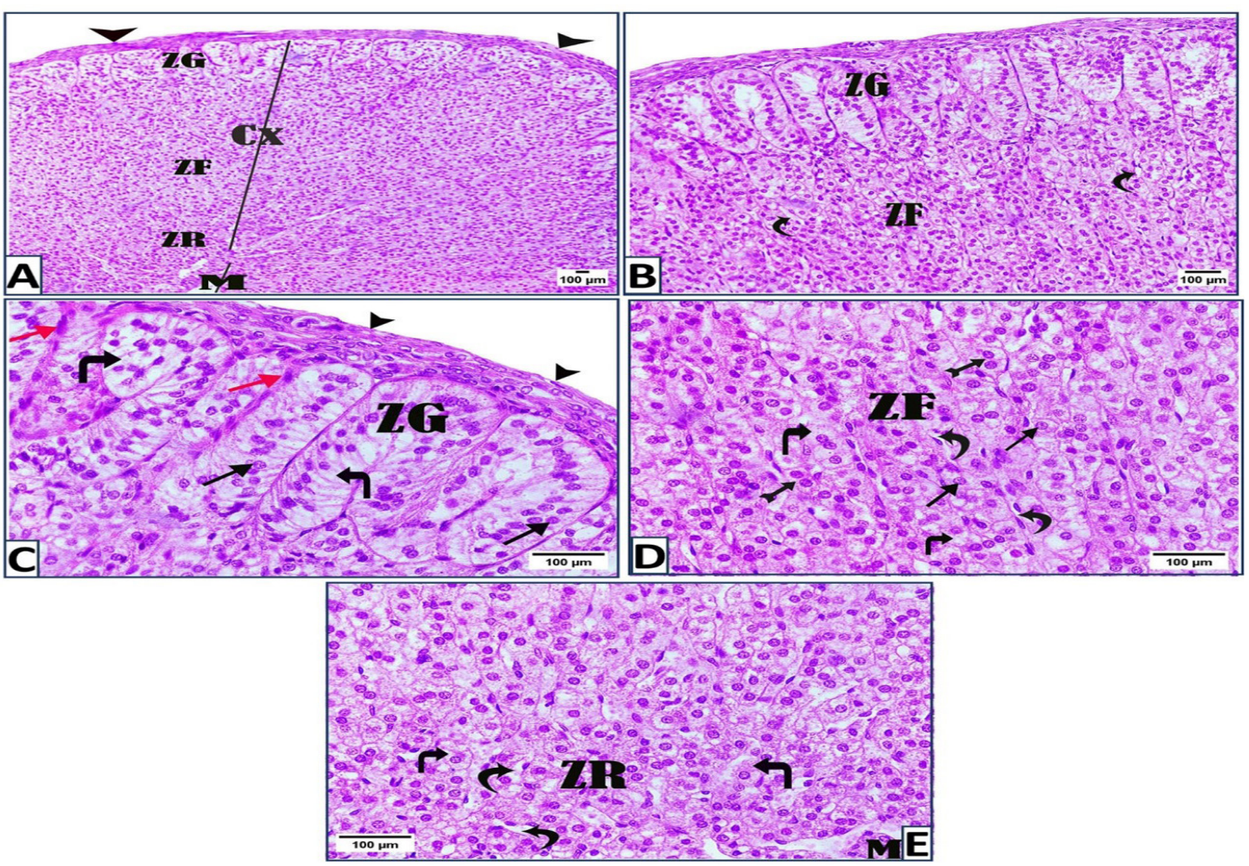

Fig. 1: Photomicrographs of H &E stained- sections of the adrenal cortex from the control group (A): showing a thin CT capsule surrounding the adrenal gland (►). The adrenal gland comprises an outer cortex (Cx) & inner medulla (M). The cortex is composed of outer zona glomerulosa (ZG), middle zona fasciculata (ZF), and inner zona reticularis (ZR). (B): The outer ZG cells are arranged in closely packed ovoid clusters and arches. Cells of ZF are arranged as straight parallel cords. Sinusoidal capillaries are noticed between the cell cords (curved arrows). (C, D): showing the arched clusters of the columnar cells of ZG separated by trabeculae (red →) having acidophilic vacuolated cytoplasm (right-angled arrows) and rounded nuclei (→). ZF cells are large polyhedral with distinct boundaries having pale acidophilic vacuolated cytoplasm (right-angled arrows) & rounded vesicular nuclei (→). Binucleated cells (bifid arrow) are also seen in ZF. (E): showing the network of the anastomosing cords of ZR cells. The cells are small polyhedral with vacuolated cytoplasm (right-angled arrows) and are separated by capillaries (curved arrows). Note the medulla (M). [H&E stain: A x100, B x200, C, D, E x400].

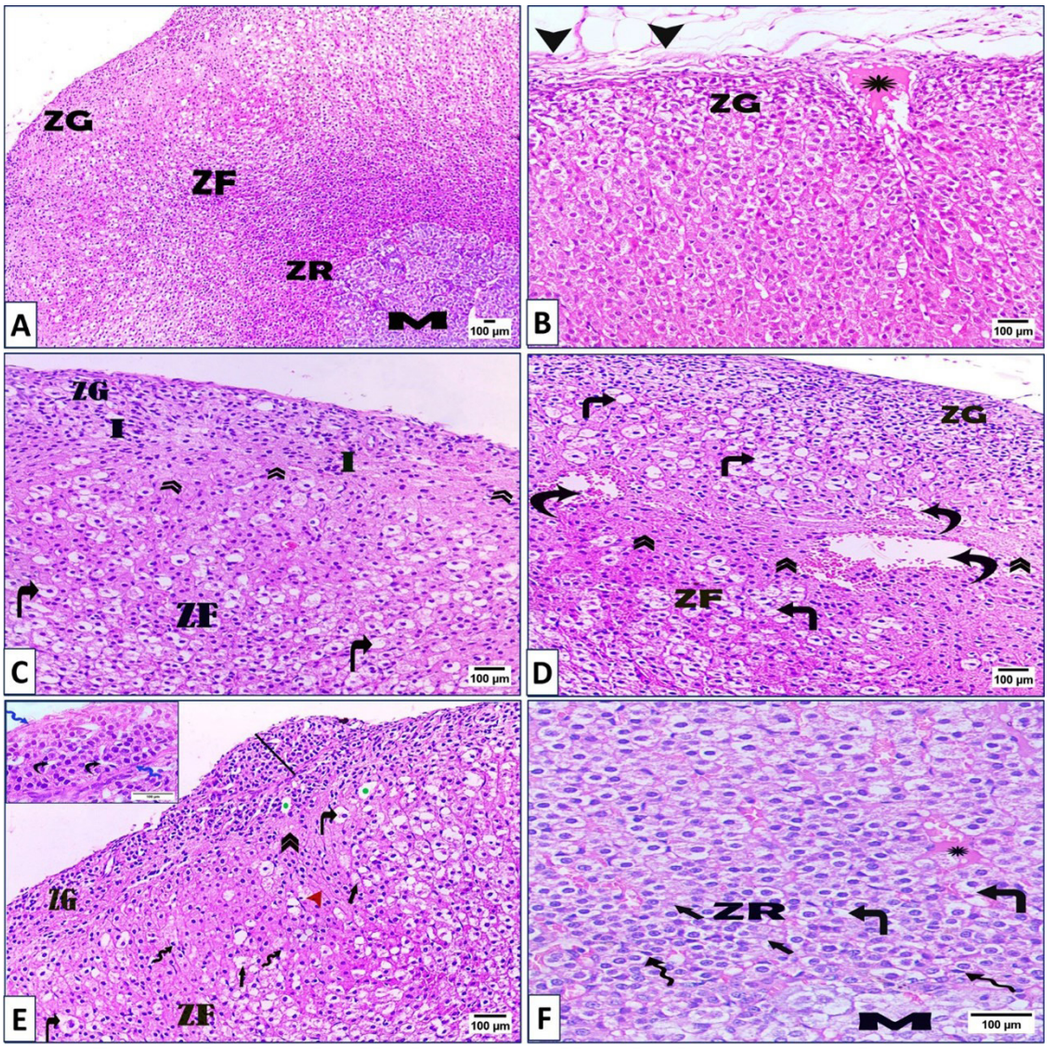

Fig. 2: Photomicrographs of H &E stained- sections of the adrenal cortex from group III (A): showing loss of the normal cellular arrangement in each zone (ZG, ZF & ZR). (B): sloughing of the CT capsule (►) and an eosinophilic homogenized material (*) between cells of ZG. (C, D, E): showing the irregular cellular arrangement of ZG & ZF, ZG's apparent hypercellularity and the intercellular spaces' widening (green •). Note the highly vacuolated cytoplasm (right-angled arrow) of ZG & ZF cells. Some cells of ZF show hyper eosinophilia with lost nuclei (red ►), faded nuclei (short arrow), and dark shrunken nuclei (wavy arrow). Homogenized eosinophilic areas with indistinct cell boundaries (»), inflammatory cellular infiltration (I) and the marked dilatation of sinusoidal capillaries with extravasation (curved arrows) are also observed. An accessory adrenocortical nodule (line) is seen. The inset shows that the cells are enveloped by a CT capsule with flattened nuclei of fibroblasts (wavy arrow) and separated by sinusoidal capillaries (curved arrow). (F): showing ZR cells having vacuolated cytoplasm (right-angled arrow). Some nuclei are dark and shrunken (wavy arrow) and others are faded (short arrow). A homogeneous eosinophilic material between cells (*) is noticed. Note the medulla (M). [H&E stain: A x100, B, C, D, E x200, F x400, Inset x1000].

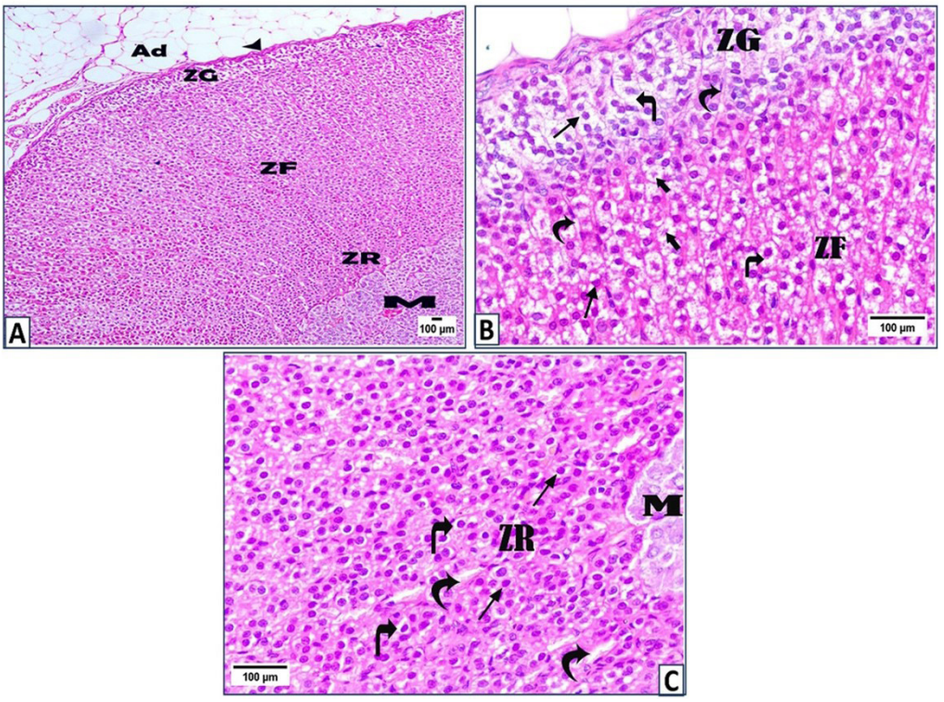

Fig. 3: Photomicrographs of H &E stained- sections of the adrenal cortex from group IV (A): showing preserved cytoarchitecture of the cortical zones (ZG, ZF &ZR). The adrenal gland is covered by a CT capsule (►) and surrounded from the outside by adipose tissue (Ad). (B): showing the cells of ZG & ZF having vacuolated acidophilic cytoplasm (right-angled arrow) and rounded nuclei (→). Few cells in ZF having faded nuclei (short arrow) are observed. (C): showing the anastomosing network of ZR cells separated by sinusoidal capillaries (curved arrow). Cells have vacuolated cytoplasm (right-angled arrow) and rounded basophilic nuclei (→). Note, the medulla (M). [H&E stain: A x100, B, C x400].

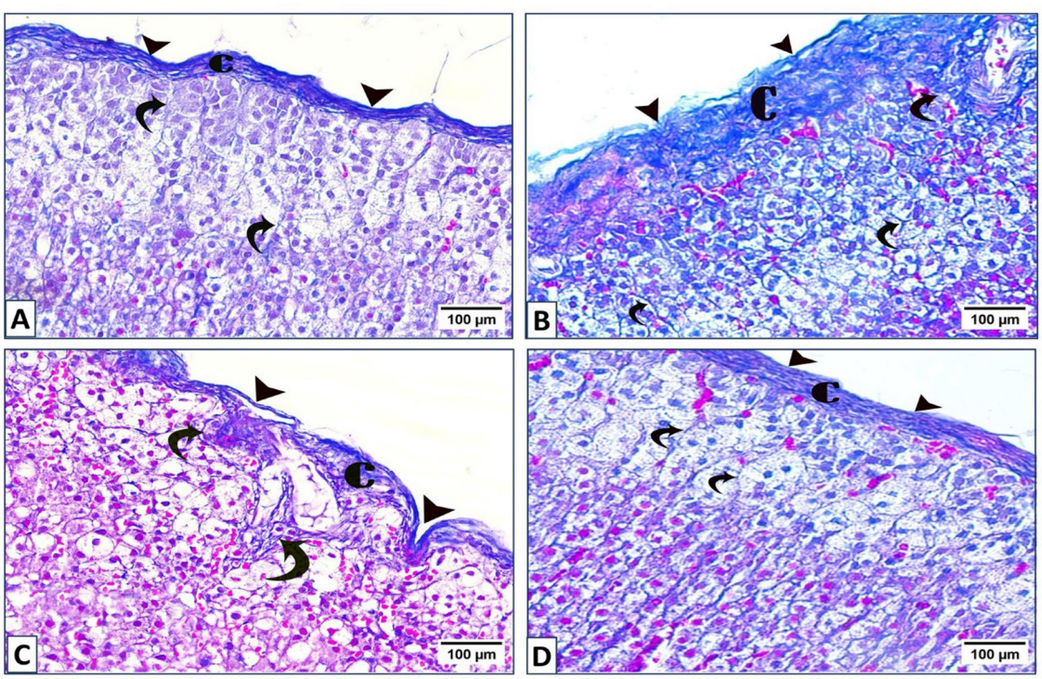

Fig. 4: Photomicrographs of Masson's trichrome stained sections of the adrenal cortex (A): from the control group showing a thin CT capsule (►). The collagen fibers (C) appear few & regular in the CT capsule and in between the adrenocorticocytes (curved arrows). (B, C): from group III showing an apparent thick, corrugated CT capsule (►) with excessive irregular collagen fibers (C) extending in-between the adrenocorticocytes (curved arrows). (D): from group IV showing fine regular collagen fibers (C) in the thin CT capsule (►) and in between the adrenocorticocytes (curved arrows). [Masson's trichrome stain: A, B, C, D x400].

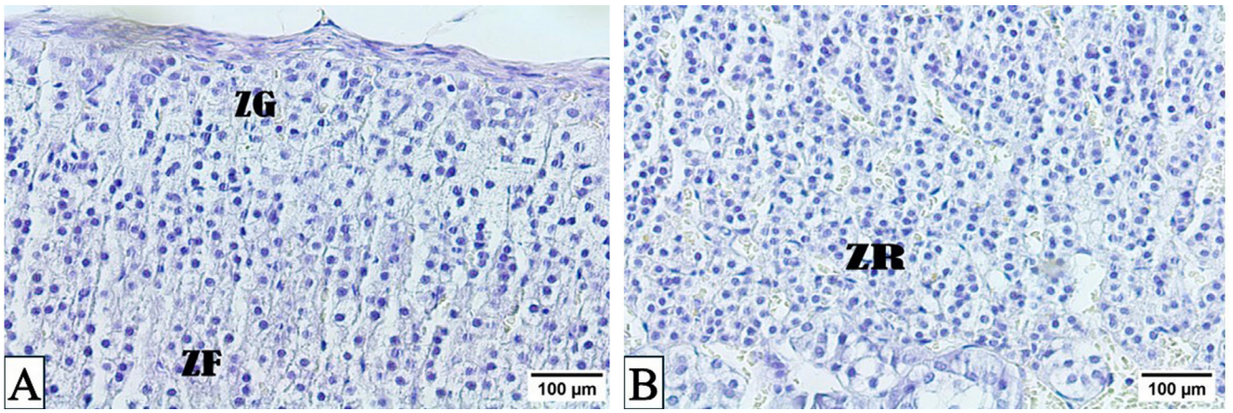

Fig. 5: Photomicrographs of the adrenal cortex of the negative control section showing (A, B): no cytoplasmic or nuclear immune reactions in ZG, ZF and ZR. [Negative control: A, B x400]

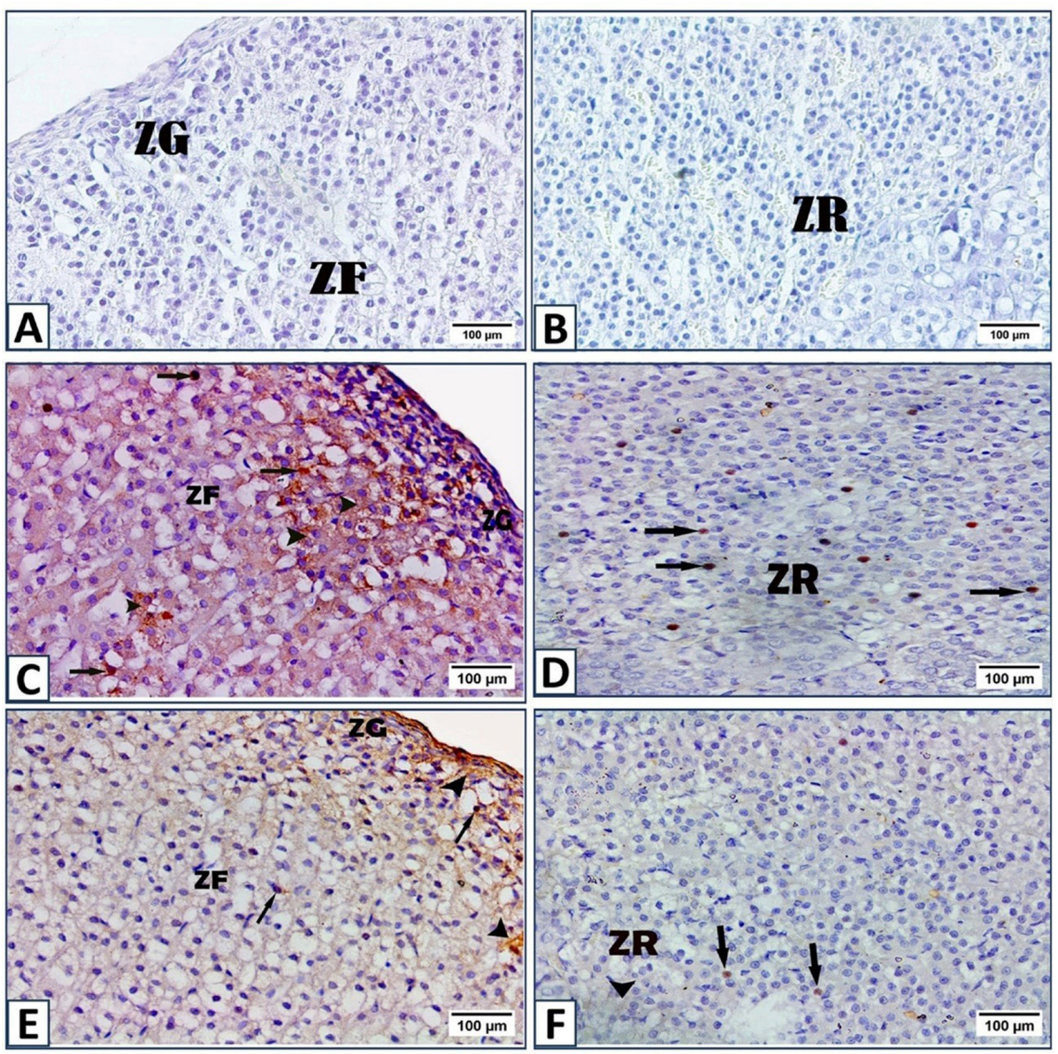

Fig. 6: Photomicrographs of cleaved caspase-3 immunostained sections of the adrenal cortex (A, B): from the control group showing no cytoplasmic or nuclear reaction in ZG, ZF & ZR. (C, D): from Group III showing an apparent intense positive cytoplasmic (►) and nuclear (→) immune reactions in ZG, ZF & ZR. (E, F): from Group IV showing a noticeable weak positive cytoplasmic (►) and nuclear (→) immune reactions in ZG, ZF & ZR. [Cleaved caspase- 3 immune staining: A, B, C, D, E, F x400].

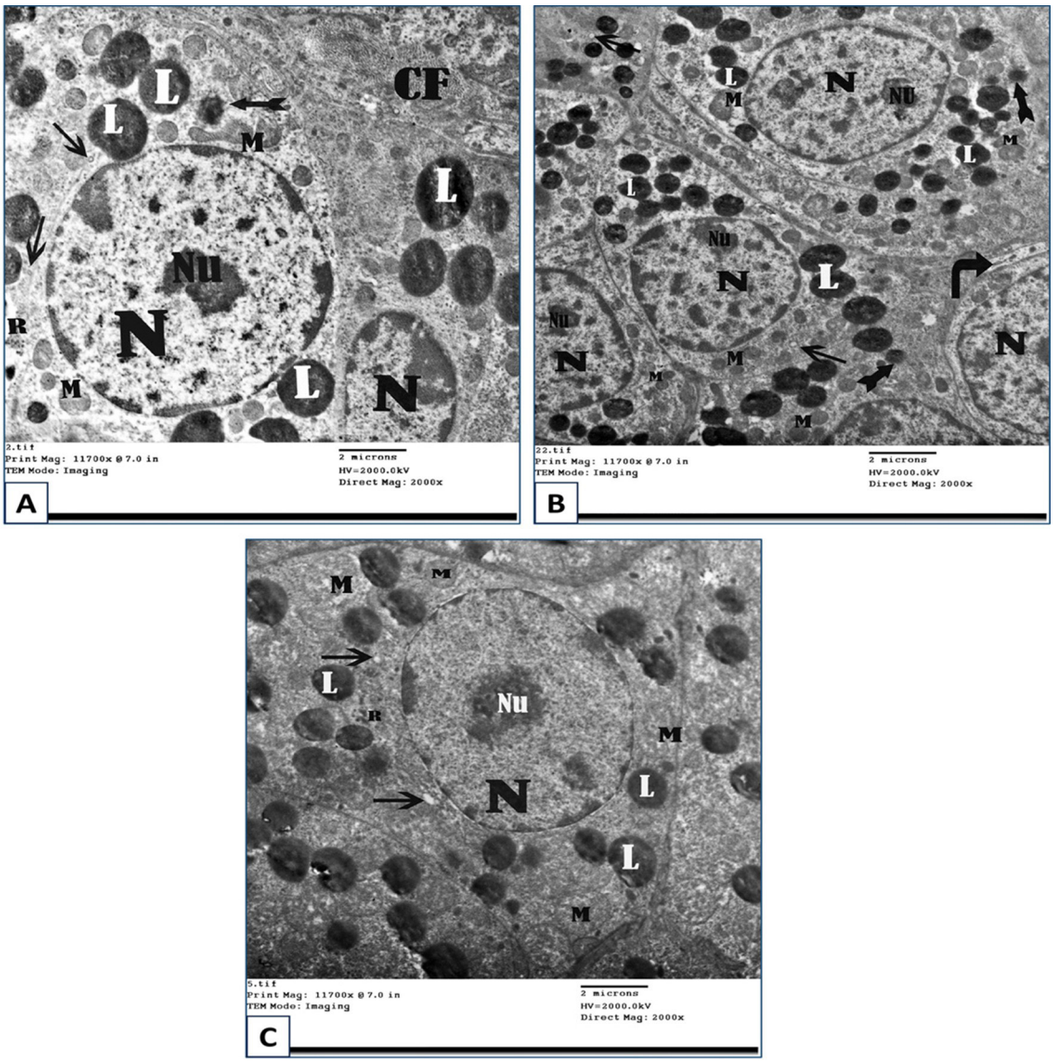

Fig. 7: TEM images of the adrenal cortex from the control group (A): showing the ZG cells with a spherical euchromatic nucleus (N) and prominent nucleolus (Nu). The cells contain mitochondria (M) varying from elongated to oval or spherical shapes, few lipid droplets (L), SER cisternae (→), free ribosomes (R), and lysosome (bifid arrows). Note the connective tissue capsule with the collagen fibers (CF). (B): showing ZF cells with spherical euchromatic nuclei (N) and prominent nucleoli (Nu). The cells contain numerous spherical mitochondria (M), numerous lipid droplets (L), SER cisternae (→), and lysosomes (bifid arrows). Note the intercellular space (right-angled arrow). (C): showing a ZR cell with a spherical euchromatic nucleus (N) and prominent nucleolus (Nu). The cells contain numerous mitochondria (M) of various sizes with tubular cristae, many lipid droplets (L), scattered ribosomes (R), and SER cisternae (→). [TEM: A, B, C x2000].

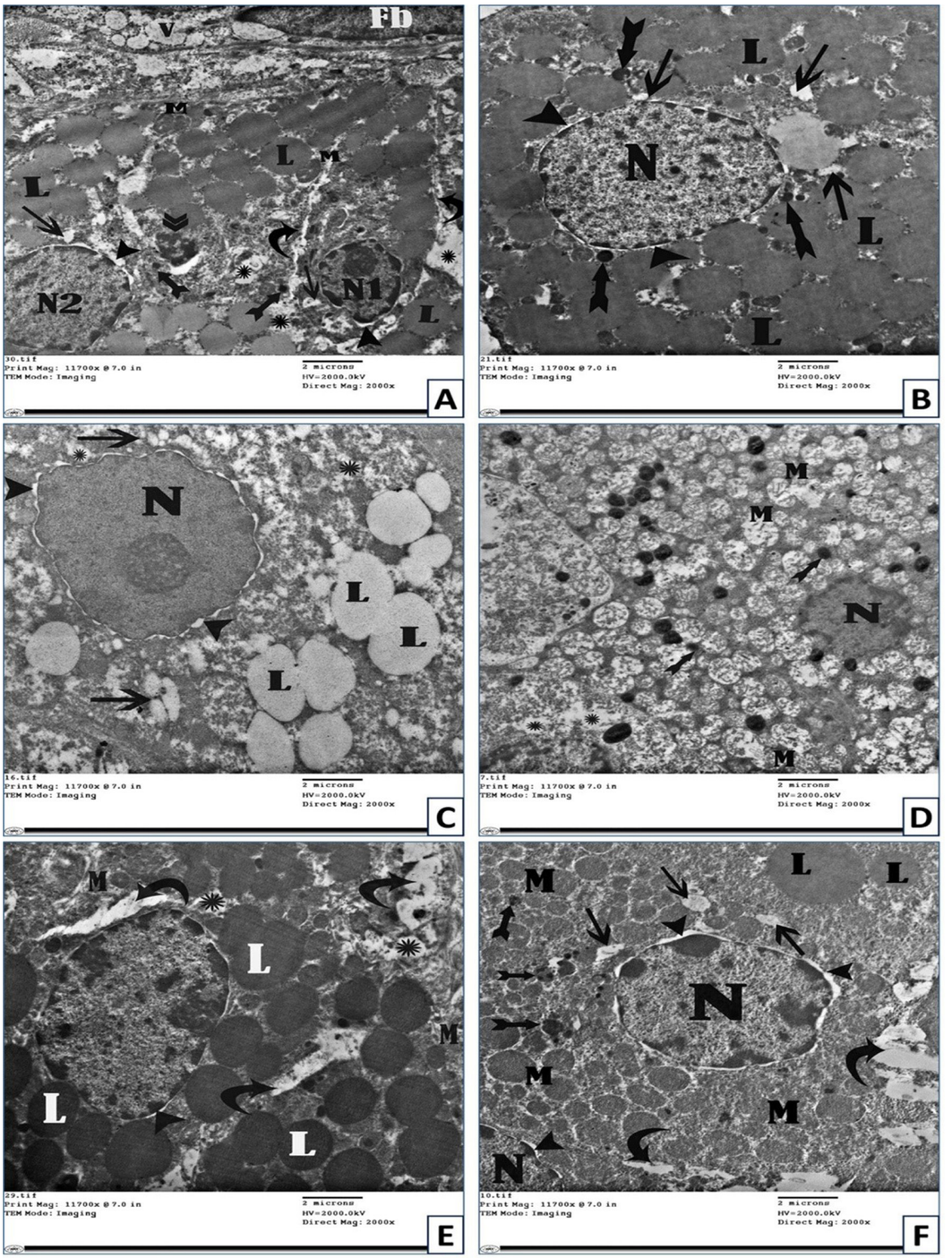

Fig. 8: TEM images of the adrenal cortex from group III (A): showing a ZG cell with a relatively shrunken irregular nucleus (N1) and another cell with a small heterochromatic nucleus (»). Focal dilatation of the perinuclear cisternae (N1&N2) (►) is observed. Small lysosomes (bifid arrows), rarified cytoplasm (*), numerous lipid droplets (L), dilatated SER (→), and small mitochondria (M) are observed. Widening of the intercellular spaces (curved arrows) is observed. Note the Fibroblast nucleus (Fb) with cytoplasmic vacuolation (V). (B, C, D): showing ZF with a spherical and slightly indented nucleus (N) with focal dilatation of the perinuclear cisterna (►). Multiple small lysosomes (bifid arrows), numerous coalesced lipid droplets (L), areas of cytoplasmic rarefaction (*), swollen vacuolated mitochondria (M) with disturbed cristae, and dilated SER (→) are observed. (E, F): showing ZR with slightly indented nuclei (N) and dilated perinuclear cisterna (►), lysosomes (bifid arrows), dilated cisternae of SER (→) and numerous variable-sized lipid droplets (L) in between the rounded mitochondria (M). Widening of the intercellular spaces (curved arrows) and large areas of rarified cytoplasm (*) are noticed. [TEM: A, B, C, D, E, F x2000].

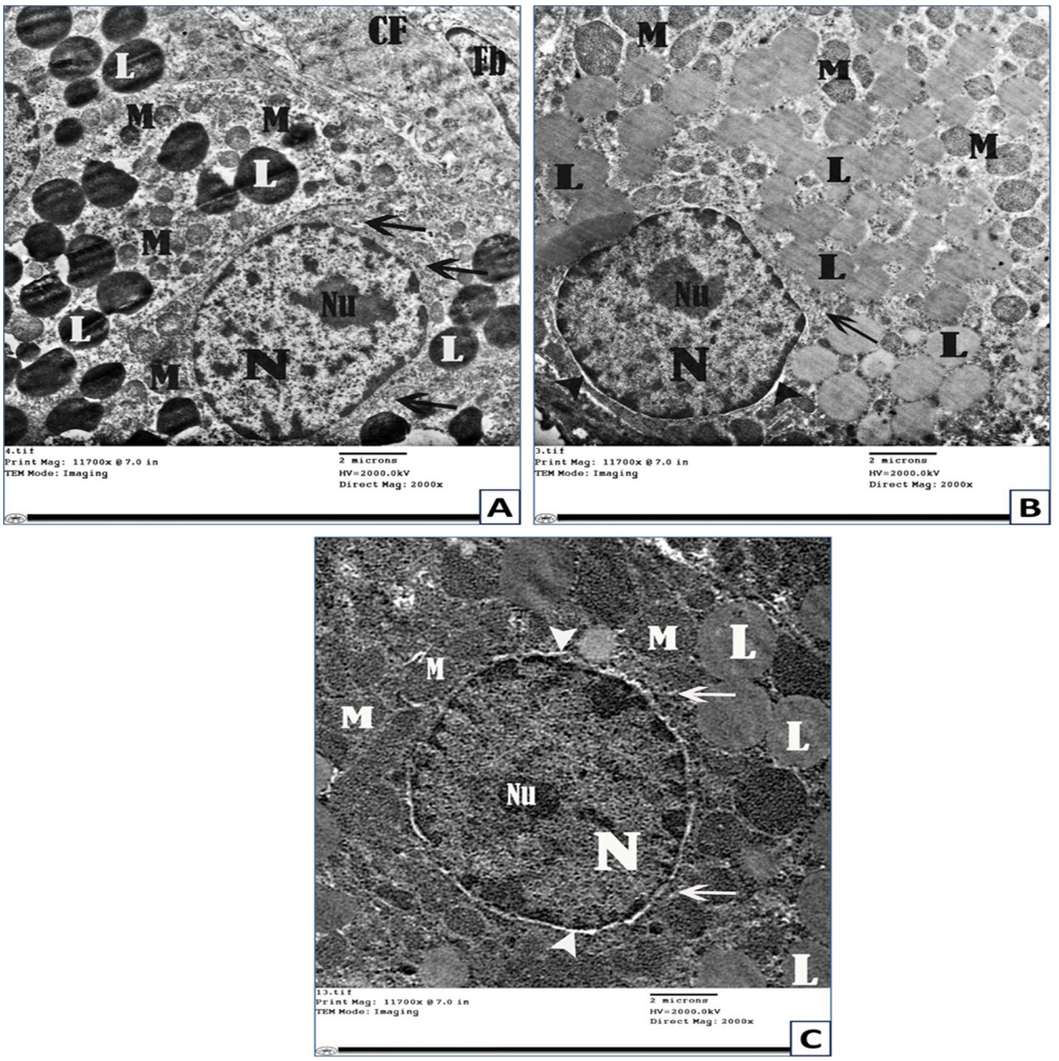

Fig. 9: TEM images of the adrenal cortex from group IV (A): the ZG cells with a spherical, regular euchromatic nucleus (N) and prominent nucleolus (Nu). The cells contain numerous mitochondria (M), lipid droplets (L), and SER cisternae (→). Note the CT capsule with the characteristic elongated nucleus of a fibroblast (Fb) and collagen fibers (CF). (B): showing a ZF cell with a spherical, slightly indented euchromatic nucleus (N) and prominent nucleolus (Nu). Mild dilatation of perinuclear cisterna (►) is noticed. The cells contain numerous mitochondria (M) of various sizes with tubular cristae, lipid droplets (L), and SER cisternae (→). (C): a ZR cell with a spherical euchromatic nucleus (N) and prominent nucleolus (Nu). Dilatation of perinuclear cisterna (►) is noticed. The cells contain numerous rounded closely packed mitochondria (M) of various sizes with tubular cristae, numerous lipid droplets (L), and SER cisternae (→). [TEM: A, B, C x2000].

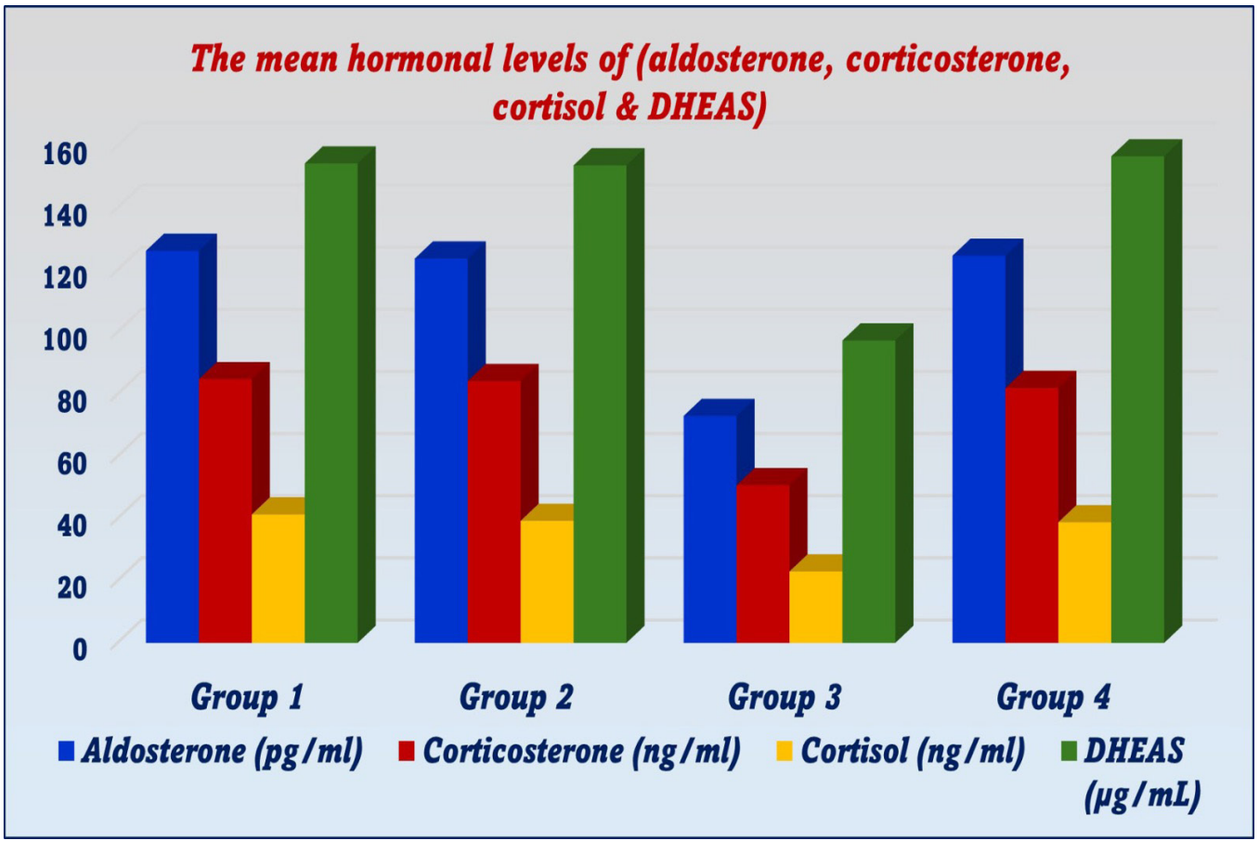

Fig. 10: Demonstrating the mean levels of aldosterone, corticosterone, cortisol & DHEA-S between the different study groups.

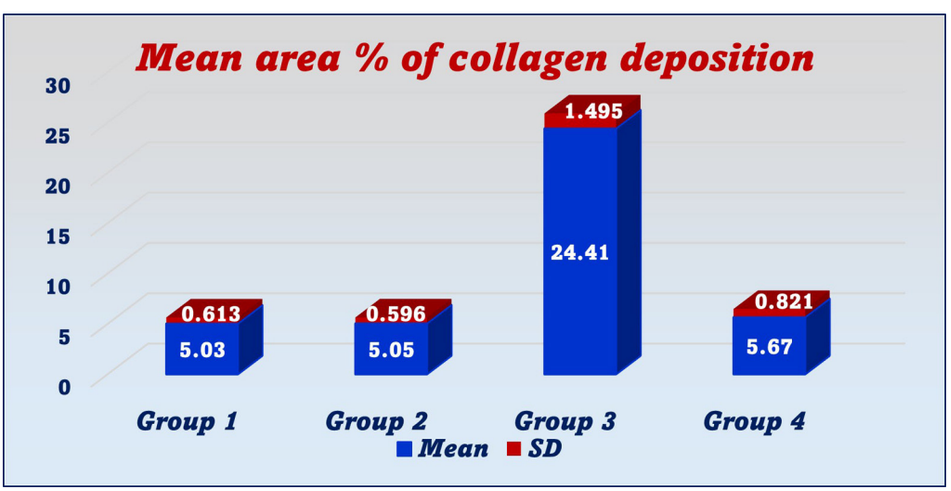

Fig. 11: Demonstrating the mean area % of collagen fibers deposition between the different study groups.

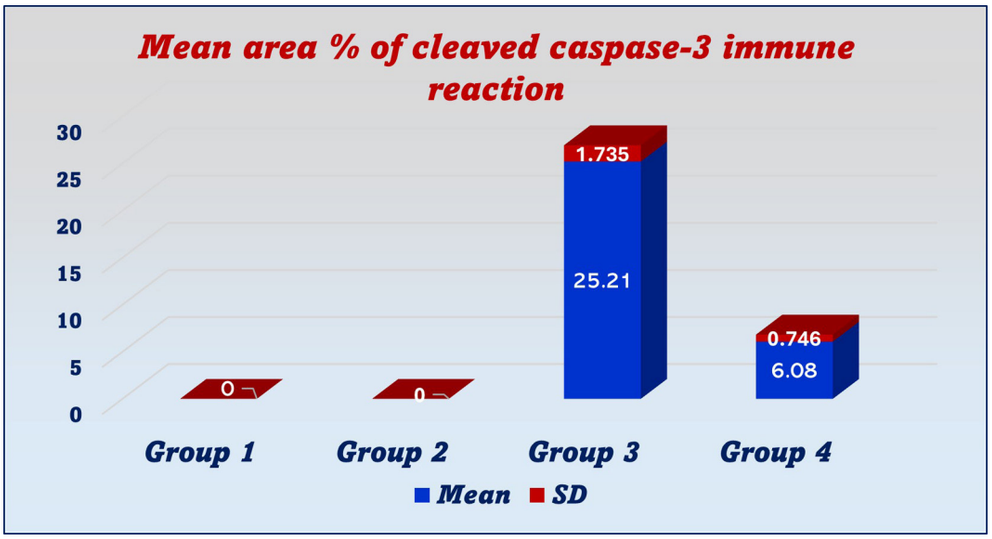

Fig. 12: Demonstrating the mean area % of cleaved caspase-3 immune reaction in the adrenal cortex between the different study groups.

Table 1: Showing the hormonal profile of the adrenal cortex in different groups using one-way ANOVA test followed by Tukey's test.

		Group I	Group II	Group III	Group IV
Aldosterone (pg/ml)	Mean ± SD	126.2±2.81[3]	123.7±2.10 [3]	73.05 ±0.72[1,2,4]	124.6 ±0.71[3]
Corticosterone (ng/ml)	Mean ± SD	84.89 ±2.90[3]	84.28 ± 2.51[3]	50.75 ±0.98[1,2,4]	82.94 ±2.26[3]
Cortisol (ng/ml)	Mean ± SD	41.34 ± 3.85[3]	39.28 ± 3.47[3]	22.99 ± 1.61[1,2,4]	38.83 ± 3.45[3]
DHEAS (µg/mL)	Mean ± SD	154.3 ±5.23[3]	153.7±5.662[3]	97.32 ± 4.50[1,2,4]	156.6 ± 4.61[3]

1: highly sig. diff. from G (I); 2: highly sig. diff. from G (II); 3: highly sig. diff. from G (III); 4: highly sig. diff. from G (IV).

Table 2: Showing the mean area % of collagen deposition in the adrenal cortex in different studied groups using one-way ANOVA test followed by Tukey's test

	Group I	Group II	Group III	Group IV
Mean ± SD	5.03±0.613[3]	5.05±0.596[3]	24.41±1.495[1,2,4]	5.67±0.821[3]

1: highly sig. diff. from G(I); 2: highly sig. diff. from G (II); 3: highly sig. diff. from G (III); 4: highly sig. diff. from G (IV).

Table 3: Showing the mean area % of cleaved caspase-3 immune reaction in the adrenal cortex in different studied groups using one-way ANOVA test followed by Tukey's test.

	Group I	Group II	Group III	Group IV
Mean ± SD	0±0[3]	0±0[3]	25.21±1.735[1,2,4]	6.08±0.746[3]

1: highly sig. diff. from G(I); 2: highly sig. diff. from G (II); 3: highly sig. diff. from G (III); 4: highly sig. diff. from G (IV).

DISCUSSION

The adrenal gland is a complicated endocrine gland that is necessary for life maintenance. It also involves major biological functions[20]. Tartrazine has been widely used in the food business, cosmetics as well as in the manufacture of medicinal capsules for vitamins and acid-reducing agents, particularly in developing nations (4.5).

According to ***Bhatt et al.***[21] and Aldaamy & Al-Zubiady[22] oxidative stress was incited by TRZ, which led to tissue damage with the generation of reactive oxygen species (ROS). They also added that oxidative stress caused by TRZ is associated with a significant increase in the concentration of oxidative stress markers such as malondialdehyde (MDA) which is the end product of lipid peroxidation and elevated nitric oxide (NO) levels. Meanwhile it causes a significant decline in the concentration of the endogenous antioxidant defense enzymes such as glutathione (GSH), superoxide dismutase (SOD), catalase (CAT) and glutathione peroxidase (GPx) due to the role of TRZ in the release of free radicals in large quantities.

In the present study, the TRZ group recorded a highly significant decline in serum corticosterone, cortisol, aldosterone, and DHEA-S levels compared to the control group. These results coincided with the results of ***Shalaby et al***[23] who observed a significant decrease in the levels of cortisol in the tramadol-treated rats and explained this drop in the hormone level to be as a result of decreased adrenal stress response, which results in adrenal inadequacy during acute illness or stress. Also, the damage in the cortical zones supported by electron and light microscopes impaired steroidogenesis.

Light microscopic examination of the adrenal cortex of Group III revealed loss of normal cellular arrangement of the three cortical zones. Cytoplasmic vacuolation, and nuclear changes as pyknosis were observed. Additionally, dilatation of sinusoidal capillaries with extravasation of blood, and eosinophilic areas were also observed.

Loss of normal cellular arrangements of the adrenal zones after TRZ administration agreed with the results of Elkelany & El Shaer[24] who noticed disturbed architecture of acinar cells of the pancreas of the TRZ group. They attributed this to TRZ-induced oxidative damage and peroxidation of lipids in the acinar cell membranes. The oxidative damage affects cellular activities by changing the cell membranes' integrity, fluidity, and physicochemical features with subsequent lipid peroxidation and cell death[25].

The present study revealed thickening of the CT capsule with intense collagen fibers deposition. This was observed in H &E and Masson's trichrome-stained sections of the TRZ group. This was also confirmed statically by the highly significant increase in the mean area % of collagen deposition versus the control group. This was in accordance with Kandeel & Sharaf Eldin[26] who detected a significant increase in the collagen fibers of the jejunal mucosa in TRZ-treated rats, and Hassanin & Shenouda[27] who detected intense collagen fibers around the acini, ducts and the blood vessels of the submandibular gland in the rats treated by TRZ. They attributed these changes to oxidation products such as lipid peroxidation stimulating the expression of α-collagen and collagen synthesis.

Consistently these observations were in the same context as ***Essawy et al.***[28] who reported an elevation in the levels of tumor necrosis factor α (TNF-α), interleukins (IL-1β & IL-6) in the TRZ treated animals. The damaged tissue releases TNF-α- inflammatory signals, stimulating fibroblast differentiation and consequently fibrosis[29].

Furthermore, inflammatory cellular infiltration was noticed in the TRZ group. This was previously noted in the study of Kandeel & Sharaf Eldin[26], who clarified that in addition to the TRZ-associated synthesis of leukotriene, TRZ might also induce pro-inflammatory responses by attracting inflammatory cells to tissues. The leukotriene TNF-α activates the nuclear factor kappa of activated B cells (NF-κB) with the production of different inflammatory chemokines. This, in turn, attracts various immune cells and starts an inflammatory response. Additionally, the released TNF-α activates the intercellular adhesion molecule 1 (ICAM-1) as well as other adhesion molecules that bring inflammatory cells[29,30].

Considering the eosinophilic homogenous material that was noticed between cells of the three adrenal zones, this coincides with the results of ***Al-Moatasem et al***[31] who observed it in the ZF of adrenal glands after aspartame administration. They explained it as accumulating protein secondary to cellular degeneration and adrenal gland dysfunction. This homogenous material may be composed of inflammatory oxidate and fibrin-like substances[32].

Concerning the accessory adrenocortical nodule observed in our results, it was described by La Perle & Dintzis[33] as an additional unique feature of the rodent adrenal cortex. The nodules of accessory cortical tissue are composed of the normal cortex and dispersed in the retroperitoneal adipose tissue or attached to the adrenal gland but separated from it by a complete fibrous capsule. Histologically, accessory adrenal tissue lacks the distinct zonal arrangement of the adrenal cortex and the central

portion of it contains dilatated capillaries, but no medullary tissue is present.

Regarding the cytoplasmic vacuolation observed in the adrenal cortical cells in group III in H &E stained sections and ultrathin sections, this goes in line with the histological findings of many investigators such as ***ElSakhawy et al.***[34] and ***Wu et al.***[35] who observed cytoplasmic vacuolation of the acinar cells in the submandibular gland, epithelial cells in the intestine, and in the hepatocytes as well as in the cerebellar neurons in rats exposed to TRZ. They attributed this finding to TRZ toxicity and explained that cytoplasmic vacuolation is a sign of cell apoptosis as cells compensate by vacuolating and swelling. They added that the vacuolar degeneration in TRZ-treated animals might be due to loss of the cell membrane's selective permeability with subsequent disturbance in the intracellular fluid and electrolytes that in turn caused dilatation of the cytoplasmic components which is the first sign of cell injury.

In the current work, dilatation and extravasation of the sinusoidal capillaries were detected. This agrees with the findings of Elkelany & El Shaer[24] who noticed dilated congested intralobular and interlobular blood vessels as well as congested blood capillaries of TRZ-treated rats as well as extravasation in the interstitial tissue of the pancreas in the same group. Congestion and interstitial hemorrhage are considered an inflammatory response to get more blood to the regions of degeneration. The congestion causes an increase in the capillary hydrostatic pressure which increases the capillary permeability in the site of inflammation that in turn can cause edema[28,29]. Meanwhile, ***Al-Moatasem et al.***[31] clarified this extravasation to the elevation of the free radicals that can cause unsaturated fatty acids peroxidation in cell membranes of the vascular tissue, with subsequent blood extravasation.

Moreover, widening of the intercellular spaces was observed in the H & E-stained sections and confirmed by ultrathin sections examination. This was in the same context with many researchers; ***Abdel-Aziz et al.***[7] within the thyroid glands of TRZ-treated rats, ***Haroun et al.***[36]in rats with acute pancreatitis induced by energy drinks, as well as Elkelany & El Shaer[24] between pancreatic lobules in TRZ- treated rats. They explained that edema might be the cause of the widening of the interlobular and interacinar septae and they attributed edema to high endogenous nitric oxide that increased the permeability of blood vessels.

The hypercellularity of ZG detected in the TRZ-treated group can be explained by the migration theory, which contends that adrenal cell regeneration starts in the outer region of the cortex and subsequently migrates from ZG to ZF to ultimately reach ZR[30]. On the other hand, ***Guo et al.***[37] declared this hypercellularity by the transformation hypothesis. It postulated that cells would first multiply in a zone between ZG and ZF before moving outward toward the capsule and inward toward the medulla.

The present work revealed homogenized eosinophilic areas in ZF with indistinct cell boundaries. This coincides with the results of ***Rahayu et al***[38] who noticed an increase in the percentage of renal tubular necrosis in the TRZ-treated animals and ***Khayyat et al***[39] who detected TRZ-induced necrosis of most hepatocytes. These necrotic areas can be explained as a result of the oxidative stress and ROS produced by TRZ that play a role in necroptosis.

In the present study, the adrenal cells of the TRZ group exhibited the presence of ballooned cells with dark nuclei alternating with cells with highly acidophilic cytoplasm and lost or pyknotic nuclei. Similar observations were reported by ***Abd El-Gawad et al.***[40] and Solaiman & Sawires[41] who stated that there were plump cells with much more cytoplasmic eosinophilia in the stressed adrenal glands.

There were marked ultrastructural alterations in the adrenal cortical cells of group III. Some cells showed shrunken nuclei and dilated perinuclear space. Other cells had dilatation of SER, swollen mitochondria, increased lipid droplets with large numerous coalesced droplets, and rarified cytoplasmic areas were also observed.

According to ***Khalaf et al.***[42] the suppression of cholesterol to pregnenolone conversion, which leads to cholesterol accumulation within the mitochondria, may be the cause of the enlargement and disturbed mitochondria. Since the SER and mitochondria are crucial to steroidogenesis, therefore, their damage was enough to prevent steroid synthesis and prevent more cholesterol buildup in the mitochondria. This hypothesis also explains our study's findings about the adrenal cortex's declining hormonal level.

Several researchers have previously observed the increased number of lipid droplets following the treatment of sodium benzoate in the hepatocytes of experimental animals and TRZ-induced hepatotoxicity, respectively[43,44].

Ultrastructurally, there was clear destruction of the cytoplasm of adrenal cortical cells with large areas of rarefaction. This was consistent with the findings of Sinha & D'Souza[45] and Bakar & Aktac[46] who observed that damage from sodium benzoate may lead to the presence of large clear spaces in hepatocytes. They clarified that the integrity of cytoplasm is important for regular intracellular

trafficking which in turn would be damaged due to cytoplasmic vacuolization.

Different nuclear changes seen in group III by light and electron microscope that were in the form of irregularity of the nuclear outlines, and shrinkage deeply stained nuclei (pyknosis). Some cells showed karyolysis presented in the form of faded chromatin, these nuclear changes as well as dilated SER and mitochondrial degenerations are considered the eminent features of apoptotic cell death[39]. This was in the same context as experimental studies performed in rats revealed that TRZ induced apoptosis in many different systems including the parotid gland[27], the kidney,[38] and the liver[39].

These nuclear changes were confirmed statistically by the highly significant increase in the mean area % of cleaved caspase-3 positive reaction (cytoplasmic and nuclear) in the cells of the three zones of the adrenal cortex of group III. Similar results were observed by ***AbdElhakim et al.***[4] in the hepatic and renal tissue of TRZ-treated rats, and ***Imam et al.***[47] in the adrenal cortex of cadmium-administered group. These results could be due to the oxidative stress of tartrazine that activates ROS-mitochondria-Casp-3 apoptosis cascades[28].

Caspase-3 is responsible for nuclear alterations in apoptosis, and it is considered the main effector caspase since both extrinsic and intrinsic pathways lead to Caspase 3 activation. The two main apoptotic pathways within a cell are the extrinsic pathway (receptor pathway) and the intrinsic one (mitochondrial pathway). The intrinsic pathway is triggered by many intrinsic factors as oxidative stress via the involvement of the mitochondria. Caspase-3 is activated by both extrinsic and intrinsic pathways[48].

In this study, giving AO concomitantly with TRZ for four weeks daily and orally preserved the morphological structure of the suprarenal cortex which appeared to a considerable extent less affected than group III. Examination by LM showed preservation of the normal histological architecture with a marked decrease in the thickness of the CT capsule compared to group III. Cytoplasmic vacuolations and nuclear changes such as karyolysis and pyknosis were markedly diminished. The congested sinusoidal capillaries were markedly reduced. This group also recorded a highly significant increase in serum aldosterone, corticosterone, cortisol and DHEA-S levels as compared to the TRZ group.

The protective properties of AO are likely attributed to its high concentration of potent antioxidants particularly: polyunsaturated and unsaturated fatty acids, polyphenols, tocopherols, sterols, and β -carotene, which are known as powerful antioxidants and provoke free radical scavenging enzyme systems. These products act by several mechanisms: scavenging of peroxy radicals, which break the peroxidation chain reaction, reducing oxidation of lipids and inhibiting the binding to apolipoproteins and subsequently preventing the modification of amino acid-Apo-B protein residue[8]. Moreover, Antioxidants present in AO are believed to prevent or delay the onset of production of ROS after lipid peroxidation observed in rats or human plasma[49].

Additionally, group IV showed a highly significant decrease in cleaved caspase-3 immune reaction versus group III. This is in accordance with the study of ***Orabi et al.***[50] who observed mild immune staining of caspase-3 within some renal tubules in the case of AO concomitant intake compared to the betamethasone group.

Ultrastructure examination of this group (group IV) revealed localized mild changes with preservation of apparently normal histo-architecture of cells. Occasionally, mild dilatation of the perinuclear cisterna with mild nuclear indentation, and few mitochondria with disrupted cristae were occasionally observed in a few cells.

These results agree with the histological findings of ***Alahmadi et al.***[51] in the kidneys of male rats of Lead-induced pathological alteration and ***Necib et al.***[52] in the liver of rats of Mercuric chloride-induced pathological alterations. They observed prominent recovery after combination with AO. ***Necib et al.***[52] also added that AO significantly increased liver GSH level, GSH-Px, and glutathione-S transferase (GST) activities as antioxidant potential thereby declining the level of lipid peroxidation. Additionally, they stated that the high level of GSH protects cellular proteins against oxidation.

From the current work, it was proved that oral administration of tartrazine induced various deleterious histo-pathological changes in the adrenal cortex and co-administration of argan oil greatly adjusted these changes.

CONCLUSION

Based on the current study and from all previously mentioned results, we found that tartrazine administration orally at a dose of 300 mg/kg daily for four weeks induces various histopathological and immunohistochemical degenerative impacts on the adrenal cortex. Co-administration of Argan oil alleviated the harmful effects of tartrazine on the adrenal cortex.

RECOMMENDATIONS

Consumption of synthetic-colored foods, especially those dyed with tartrazine, should be limited. Natural yellow food coloring such as saffron or turmeric powder should be used as an alternative to tartrazine. Argan oil supplementation is recommended as a potent antioxidant agent. We recommend more research to study the effect of tartrazine on the adrenal cortex and adrenal medulla from the pharmacological and toxicological points of view to get a better understanding of the mechanism of occurrence of these effects and the possibility of recovery.

CONFLICT OF INTERESTS

There are no conflicts of interest.

REFERENCES

1. **Oplatowska-Stachowiak M and Elliott CT (2017):** Food colors, Existing and emerging food safety concerns. Critical Reviews in Food Science and Nutrition (CRFSN)). 57(3):524-548.

2. **Zeece M. (2020):** Food colorants. In: An Introduction to the Chemistry of Food, 1st edition: Academic Press, Elsevier. Chapter 8, P:313–344.

3. **Benkhaya S; M'rabet S and El Harfi A (2020):** Classifications, properties, recent synthesis, and applications of azo dyes. Heliyon, Elsevier Limited. 6(1): 1–26.

4. **Abd-Elhakim YM; Hashem MM; El-Metwally AE, *et al.* (2018):** Comparative haemato-immunotoxic impacts of long-term exposure to tartrazine and chlorophyll in rats. International Immunopharmacology. 63: 145–154.

5. **Erdemli Z; Altinoz E and Erdemli ME, *et al.* (2021):** Ameliorative effects of crocin on tartrazine dye–induced pancreatic adverse effects: a biochemical and histological study. Environmental Science & Pollution Research International (ESPRI). 28(2): 2209–2218.

6. **Al Reza MSA; Hasan MM; Kamruzzaman M, *et al.*** (2019): Study of a common azo food dye in mice model: Toxicity reports and its relation to carcinogenicity. Nutrition & Food Science (NFS). 7(2):667-677.

7. **Abdel-Aziz HM; Alazouny ZM and Abdelfadeel KF, *et al.* (2019):** Effect of tartrazine on the thyroid gland of male rat and ameliorating role of curcumin (histological and immunohistochemical study). Journal of Biochemistry & Cell Biology (JBCB). 2(1):111-120.

8. **Charrouf Z and Guillaume D (2018):** The argan oil project: going from utopia to reality in 20 years. EDP Sciences. 25 (2):209-214.

9. **El Abbassi A; Khalid N and Zbakh H, *et al.* (2014):** Physicochemical characteristics, nutritional properties, and health benefits of Argan oil: A review. Critical Reviews in Food Science and Nutrition (CRFSN). 54(11):1401–1414.

10. **Sour S; Belarbi M and Khaldi D, *et al.* (2012):** Argan oil improves surrogate markers of CVD in humans. British Journal of Nutrition. 107(12): 1800-1805.

11. **Berrada Y; Settaf A and Baddouri K, *et al.* (2000):** Experimental evidence of an antihypertensive and hypocholesterolemic effect of argan oil. Argania Sideroxylon. Therapie. 55(3): 375-378.

12. **Boussada M; Lamine JA and Bini ID, *et al.* (2017):** Assessment of a sub-chronic consumption of tartrazine (E102) on sperm and oxidative stress features in Wistar rat. International Food Research Journal (IFRJ). 24(4): 1473-1481.

13. **Ghasi S; Umana I and Ogbonna A, *et al.* (2020):** Cardioprotective effects of animal grade piperazine citrate on isoproterenol-induced myocardial infarction in Wistar rats: Biochemical and histopathological evaluation. African Journal of Pharmacy and Pharmacology (AJPP). 14(8): 285-93.

14. **Dey P. (2022):** Hematoxylin and Eosin Stain of the Tissue Section. In: Basic and Advanced Laboratory Techniques in Histopathology and Cytology, 1st edition: Springer, Singapore. Chapter 8, P:72.

15. **Leonard AK; Loughran EA; Klymenko Y, *et al.* (2018):** Methods in Cell Biology, Methods for the visualization and analysis of extracellular matrix protein structure and degradation. Academic Press. 143 (4): 79-95.

16. **Magaki S; Hojat SA and Wei B, *et al.* (2019):** An Introduction to the Performance of Immunohistochemistry. Methods in Molecular Biology. 1897(25): 289-298.

17. **Cheville NF and Stasko J (2014):** Techniques in electron microscopy of animal tissue. Veterinary Pathology. 51(1):28-41.

18. **Jensen EC. (2013):** Quantitative Analysis of Histological Staining and Fluorescence Using Image J. Anatomical Record. 296(3):378-81.

19. **Dawson B and Trapp RG. (2020):** Statistical Methods for Multiple Variables. In: Basic and Clinical Biostatistics, 5th ed: New York, McGraw-Hill Education/Medical. Chapter 10, P:190–220.

20. **Sakr SM and Sabry SA (2016):** Midazolam impact on the ultrastructural characteristic of mice adrenal cortex. Merit Research Journal of Medicine and Medical Sciences (MRJMMS). 4(1): 059–067.

21. **Bhatt D; Vyas K and Singh S, *et al.* (2018):** Tartrazine induced neurobiochemical alterations in rat brain sub-regions. Food and Chemical Toxicology (FCT). 113: 322-327.

22. **Aldaamy, AMZ and Al-Zubiady, NMH (2021):** Study on the toxic effect of tartrazine pigment on oxidative stress in male albino rats. Biochemical & Cellular Archives. 21(1): 1021-1026.

23. **Shalaby AM; Aboregela AM and Alabiad MA, *et al.* (2020):** Tramadol Promotes Oxidative Stress, Fibrosis, Apoptosis, Ultrastructural and Biochemical alterations in the Adrenal Cortex of Adult Male Rat with Possible Reversibility after Withdrawal. Microscopy and Microanalysis. 26(3):509-523.

24. **Elkelany M and El Shaer D (2023):** Histological and Immunohistochemical Assessment of the Impact of Geraniol on Tartrazine Induced Histopathological Alterations in The Exocrine Pancreas of Adult Male Albino Rat. Egyptian Journal of Histology (EJH). 46(4): 2017-2036.

25. **Zafar M; Ali S and Beenish H, *et al.* (2021):** Curcumin's neuroprotective efficacy against tartrazine induced Nissl rim alterations in adult male rats' motor cortex. Journal of Islamic International Medical College (JIIMC). 16 (3):180-184.

26. **Kandeel S and Sharaf Eldin HEM (2021):** The possible ameliorative effect of manuka honey on tartrazine-induced injury of the jejunal mucosa with the role of oxidative stress and TNF-alpha: histological and morphometric study. Egyptian Journal of Histology (EJH). 44(1):48-60.

27. **Hassanin HM and Shenouda MBK (2023):** Histological and Immunohistochemical Study of Tartrazine Effect on The Adult Albino Rat Parotid Gland and The Possible Protective Role of Omega-3 Fatty Acids. Egyptian Academic Journal of Biological Sciences (EAJBSC), (D-Histology and histochemistry). 15(1):17-38.

28. **Essawy AE; Mohamed AI and Ali RG, *et al.* (2022):** Analysis of Melatonin Modulating Effects Against Tartrazine- Induced Neurotoxicity in Male Rats: Biochemical, Pathological & Immunohistochemical Markers. Neurochemical Research. 48:131–141.

29. **Lau KS; Cortez-Retamozo V and Philips SR, *et al.* (2012):** Multi-scale in *vivo* systems analysis reveals the influence of immune cells on TNF-α-induced apoptosis in the intestinal epithelium. PLOS Biology. 10(9): 1-14.

30. **Ruder B; Atreya R and Becker C (2019):** Tumour necrosis factor alpha in intestinal homeostasis and gut-related diseases. International Journal of Molecular Sciences (IJMS). 20(8): 1887-1895.

31. **Al-Moatasem MA; Helmy DHA and Mostafa SK, *et al.* (2024):** The Protective Effect of L-Arginine against Aspartame-Induced Toxicity on Adrenal Cortex of Adult Male Albino Rats: Histological, Immunohistochemical, and Biochemical Study. Egyptian Journal of Cell & Tissue Research (EJCTR). 2(1):58-91.

32. **Paraskevi A; Theodoropoulos G and Papaconstantinou I, *et al.* (2012):** Circulating MicroRNA in inflammatory bowel disease. Journal of Crohn's & Colitis. 6(9):900-904.

33. **La Perle KMD and Dintzis SM (2018):** Endocrine System. In: Comparative Anatomy and Histology: A Mouse, Rat, and Human Atlas, 2nd edition: Academic Press, Elsevier. Chapter 15, P: 251-273.

34. **El-sakhawy MA; Mohamed DW and Ahmed YH (2019):** Histological and immunohistochemical evaluation of the effect of tartrazine on the cerebellum, submandibular glands, and kidneys of adult male albino rats. Environmental Science and Pollution Research (ESPR). 26(10):9574–9584.

35. **Wu L; Xu Y and Lv X, *et al.* (2021):** Impacts of an azo food dye tartrazine uptake on intestinal barrier, oxidative stress, inflammatory response and intestinal microbiome in crucian carp (Carassius auratus). Ecotoxicology and Environmental Safety. 223:112551.

36. **Haroun H; Mohamed E and El Shahat AE, *et al.* (2020):** Adverse effects of energy drink on rat pancreas and the therapeutic role of each of bone marrow mesenchymal stem cells and nigella Sativa oil. Folia Morphologica. 79(2):272-279.

37. **Guo Y; Zhang L and Yao X, *et al.* (2019):** Effects of nitric oxide on steroidogenesis and apoptosis in goat luteinized granulosa cells. Theriogenology. 126: 55-62.

38. **Rahayu MS; Wahyuni S and Fitriani I, *et al.* (2022):** Effect of tartrazine on blood urea nitrogen, creatinine levels, and renal tubular necrosis in adult male Wistar rats (Rattus norvegicus): an experimental study. Bali Medical Journal. 11(3): 1755-1759.

39. **Khayyat L; Essawy A and Sorour J, *et al.* (2017):** Tartrazine induces structural and functional aberrations and genotoxic effects in *vivo*. Peer J Inc. 5(8): e3041.

40. **Abd El-Gawad FA; Zaki SM and El-Shaarawy EA, *et al.* (2016):** Histological and histomorphometric reorganization of the adrenal cortex of adolescent male albino rat following exposure to stress. Medical Journal of Cairo University (MJCU). 84 (1): 1107 - 1112.

41. **Solaiman AA and Sawires SKS (2019):** Histological Study of the Effect of Tributyltin on the Adrenal Cortical Cells of Adult Male Albino Rats. Egyptian Journal of Histology (EJH). 43(1):104-121.

42. **Khalaf HA; Ghoneima FM and Arafat EA, *et al.* (2017):** Histological effect of nicotine on adrenal zona fasciculata and the effect of grape seed extract with or without withdrawal of nicotine. Journal of Microscopy and Ultrastructure (JMU). 5(3):123–131.

43. **Khidr B; Makhlouf M and Ahmed S (2012):** Histological and ultrastructural study on the effect of sodium benzoate on the liver of adult male albino rats. Assiut University Journal of Zoology. 41(1):11–39.

44. **Saxena B and Sharma S (2015):** Food color induced hepatotoxicity in Swiss albino rats, Rattus norvegicus. Toxicology International. 22(1):152-157.

45. **Sinha R and D'Souza D (2010):** Liver cell damage caused due to sodium benzoate toxicity in mice. International Journal of Biochemistry and Biotechnology (IJBB). 6(4):549–554.

46. **Bakar E and Aktac T (2014):** Effects of sodium benzoate and citric acid on serum, liver, and kidney tissue total sialic acid levels: an ultrastructural study. Journal of Applied Biological Sciences (JABS). 8(2):9–15.

47. **Imam RA; Motawei AG and Abd Algaleel WA (2020):** Cadmium-induced adrenal cortical autophagy in rats: possible modulation by sildenafil. Folia Morphol (Warsz). 79(4):709-719.

48. **Asadi M; Taghizadeh S and Kaviani E, *et al.* (2021):** Caspase-3: Structure, function, and biotechnological aspects. Biotechnology & Applied Biochemistry. 69: 1633–1645.

49. **Essadek S; Bouchab H and El Kebbaj R, *et al.* (2022):** Effects of a Short-Term Lipopolysaccharides Challenge on Mouse Brain and Liver Peroxisomal Antioxidant and β-oxidative Functions: Protective Action of Argan Oil. Pharmaceuticals. 15(4): 465-485.

50. Orabi SH; Allam TS; Shawky SM, *et al.* (2020): The antioxidant, anti-apoptotic, and proliferative potency of Argan oil against betamethasone-induced oxidative renal damage in rats. Biology. 9(11):1–17.

51. Alahmadi AA; Rabah SO and Al-Baqami NM, *et al.* (2018): Physiological and Histopathological Effect of Argan (Argania spinosa L.) Seed Oil on Kidney Male Rats Exposed to Lead. World Applied Sciences Journal (WASJ). 36 (6): 733-741.

52. Necib Y; Bahi A and Zerizer S (2013): Argan oil (Argania spinosa L) Provides protection against mercuric chloride-induced oxidative stress in rat Albinos Wistar. International Journal of Basic & Applied Sciences (IJBAS). 2 (1): 73-80.

تأثير التارترازين على قشرة الغدة الكظرية في ذكرالجرذ الأبيض البالغ والدور الوقائي المحتمل لزيت الأرجان (دراسة هستولوجية، بيوكيميائية حيوية)

أميرة إبراهيم المصري[١]، جيهان محمد سليمان[٢]، صديقة محمد توفيق[٢] و سوزان السيد أبو النصر[٢]

قسم الهستولوجيا وبيولوجيا الخلية، كلية الطب، [١]جامعة السويس، [٢]جامعة طنطا، مصر

المقدمة: يمثل التارترازين أحد عوامل التلوين الأكثر استخدامًا في الأغذية والصناعات الدوائية. أدى الاستخدام الشاسع للتارترازين إلى اضطرابات متعددة الأنظمة في القوارض والبشر. تبين أن زيت الأرجان له خصائص مضادة للأكسدة.

الهدف من البحث: دراسة تأثير التارترازين على قشرة الغدة الكظرية في ذكر الجرذ الأبيض البالغ والدور الوقائي المحتمل لزيت الأرجان.

المواد وطرق البحث: تم تقسيم أربعين من ذكور الجرذان البيضاء البالغة إلى أربع مجموعات بالتساوي. المجموعة الأولى كانت المجموعة الضابطة. المجموعة الثانية تلقت زيت الأرجان بجرعة قدرها 5 مل/كجم بالفم مرة واحدة يومياً لمدة أربعة أسابيع. المجموعة الثالثة تلقت التارترازين بجرعة قدرها 300 ملجم / كجم مذابة في 1 مل من الماء المقطر بالفم مرة واحدة يومياً لمدة أربعة أسابيع. تلقت المجموعة الرابعة التارترازين بالتزامن مع زيت الأرجان بنفس الجرعة والطريقة مثل المجموعتين الثانية والثالثة. تم جمع عينات الدم لتحليل مستويات هرمونات الألدوستيرون، الكورتيكوستيرون، الكورتيزول وDHEA-s، وتم تجهيز الغدد الكظرية لإجراء الدراسات النسيجية والهستوكيميائية المناعية ودراسات المجهرالالكترونى النافذ.

النتائج: كشفت المجموعة الثالثة عن بنية نسيجية مضطربة لمناطق قشرة الغدة الكظرية الثلاث مع ترسب الكولاجين المكثف في كبسولة النسيج الضام وبين الخلايا في المقاطع االمصبوغة بالماسون ثلاثية الألوان مع رد فعل مناعي إيجابي مكثف للكاسبيز المشقوق 3. كشفت الفحوصات المجهرية الإلكترونية عن وجود نوى غير منتظمة متباعدة مع تمدد الفراغ المحيط بالنواة ، والميتوكوندريا المنتفخة. تناول زيت الأرجان قد حسَّن النتائج الهستولوجية والهستوكيميائية مناعية والكيميائية الحيوية والمورفومترية.

الاستنتاج: أظهرت نتائج الدراسة الحالية أن التناول المتزامن لزيت الأرجان مع التارترازين حسَّن بشكل كبيرمن التأثيرات الضارة للتارترازين على بنية قشرة الغدة الكظرية.